18TH WORLD CONFERENCE ON EARTHQUAKE ENGINEERING
WCEE2024
MILAN

MILAN, ITALY
30TH JUNE - 5TH JULY 2024

www.wcee2024.it

MULTI-HAZARD RISK AND RESILIENCE ASSESSMENT FOR THE EGNATIA ODOS HIGHWAY IN GREECE

A. Chatzidaki[1], D. Vamvatsikos[2], M. Loli[3] & A. Tsatsis[3]

[1] National Technical University of Athens, Athens, Greece, cakrivi@central.ntua.gr

[2] National Technical University of Athens, Athens, Greece

[3] Grid Engineers, Athens, Greece

Abstract: *Risk and resilience are assessed for the Metsovo-Panagia segment of the Egnatia highway in Greece, focusing on the seismic and the wind hazard. This segment comprises steep slopes, bridges and the operator control building that are vulnerable to the seismic hazard as well as an ensemble of sign-support structures over several kilometers of the highway that are exposed to environmental conditions, thus being susceptive to fatigue damage under wind loading. The aim is to develop a tool for pre-event risk assessment and rapid post-event inspection of critical road infrastructure by combining hazard, vulnerability, and sensor information to predict the resulting consequences. A component-based approach is adopted for the critical highway assets while asset interdependencies are considered to assess the system-level consequences for the entire highway. These are quantified in terms of direct monetary losses and downtime as well as actions that the road operator shall take until repair actions have finished, i.e., number of closed lanes and the allowable speed limit in the remaining open ones. This allows tracing back the consequences after an event to individual components/assets and can help road operators establish inspection prioritization protocols and manage associated incidents, facilitating the rapid assessment of the state of the highway and optimal recovery to full functionality.*

1 Introduction

Nowadays road operators are facing the challenge of efficient maintenance and operation of road infrastructure networks as well as rapid inspection and efficient recovery after catastrophic events. To this scope, researchers have focused on assessing risk and resilience either on an asset-level, i.e., for the critical highway assets such as bridges and tunnels (e.g., Dong and Frangopol 2015), as well as for the entire highway network. Risk assessment aims to assess the probability (or frequency) of occurrence of an undesirable event as well as the associated consequences (e.g., Kappos et al. 2014), while resilience assessment goes a step further as it incorporates the dimension of post-event time and aims to assess the follow-up to a failure, i.e., to quantify the ability of the system to recover after an event. Several approaches aim to assess risk and resilience for infrastructure networks, either focusing on a single hazard e.g., seismic (e.g., Werner et al. 2000, Kiremidjian et al. 2007, Costa et al. 2020), weather (e.g., Markolf et al. 2019), or in a multi-hazard environment. Conceptual views of multi-hazard risk and resilience assessment of infrastructure networks have been offered (e.g., Argyroudis et al. 2020), while quantitative approaches have also been proposed (e.g., Ayyub et al. 2007, Faturechi and Miller-Hooks 2014). Still, the definition and application of a practical approach for multi-hazard

risk and resilience assessment that allows quantifying the follow-up to a failure at every step of a system's recovery back to full functionality, remains a challenge.

In our case, the HAPI multi-hazard risk and resilience assessment framework is developed and is demonstrated using the Metsovo-Panagia segment of Egnatia Odos as the case-study, focusing on the seismic and the wind hazards. This segment has a total length of ~16km and comprises four lanes in total, two per travel direction. The aim is to develop a tool for pre-event risk assessment and rapid post-event inspection of critical road infrastructure by combining hazard, vulnerability, and (if available) sensor information to predict the resulting consequences. The proposed framework allows tracing back the consequences after an event to individual components/assets and can help road operators establish inspection prioritization protocols and manage associated incidents, facilitating the rapid assessment of the state of the highway and optimal recovery to full functionality. The outcomes are integrated into the holistic decision support tool that aims to facilitate informed decisions of the stakeholders before and after potentially catastrophic events and can help the road operators efficiently inspect, maintain, and safely operate road infrastructure networks, efficiently mitigating and managing risks.

2 HAPI risk and resilience assessment framework

The HAPI risk and resilience assessment framework (Vamvatsikos and Chatzidaki, 2022) relies on the basic principles that are employed for any practical risk assessment approach, i.e., (i) Stochastic Event Set (SES) of potential event realizations, (ii) the associated Intensity Measure (IM) fields that describe the spatially correlated IM values at each location of interest, (iii) the exposure model describing the assets at risk, and (iv) the asset vulnerability functions. By employing a large-scale Monte Carlo analysis, at a minimum loss curves and loss maps can be derived that provide the overall statistics, while detailed realizations of damage and loss for all assets can also be quantified. These fundamental quantities are combined to allow us to conduct both long-term and short-term assessments with ready fusion of sensor input.

Long-term pre-event assessment

In the long-term pre-event assessment phase, the performance of the critical assets is assessed for all hazards affecting them, thus damage and associated consequences are quantified, the latter in terms of cost, downtime, and actions that the road operator shall take, i.e., close any lanes and/or reduce the speed limit in the open ones. This process requires modelling each critical asset either in detail, e.g., by employing a complex model or a surrogate one and subjecting it to analyses under a suite of recordings that represent the hazard to which the asset is vulnerable. For instance, an asset vulnerable to the seismic hazard is subjected to a set of ground motion records that are consistent to the site-specific seismic hazard, while assets vulnerable to wind actions are subjected to stochastic wind time histories. Based on the analysis results, "all" potential damage and consequence realization scenarios are assessed, for all perils affecting the asset. The ensemble of damage and consequence scenarios for all assets and hazards comprise the asset impact database.

Within the pre-event phase, SESs are also developed representing the hazards of interest. Each SES comprises a number of IM fields that provide spatially correlated IM values for single events and allow assessing concurrent damage and consequences for more than one spatially distributed assets. Thus, by combining them with individual asset scenarios, "all" potential damage and consequence scenarios for the entire highway can be determined. This operation is time-consuming and employs the best currently-available data to arrive at a set of different potential future outcomes for the highway; thus it is only performed once. The individual scenarios can be aggregated to assess the long-term damage and consequence data both on an asset-basis and for the entire highway. The pre-event framework is presented in Figure 1a.

Short-term trans/post-event assessment

In the trans-event phase, where the event has just happened (e.g., earthquake) or is presently unfolding (e.g., an on-going flood), sensor information can be employed to prune down the large set of potential scenarios that have been generated in the pre-event long-term assessment mode and provide a near-real-time assessment, as schematically presented in Figure 1b. To this scope, different types of sensors can be employed, namely: (i) Type I sensors that provide information on the hazard (e.g., seismographs, weather stations or flood height meters). Such sensors offer information on the actual values of the IM experienced at each site of interest and can be used to prune down the hazard scenarios; (ii) Type II sensors that provide information on the assets' response (e.g., accelerometers and strain gages) and can be employed for finding the closest asset impact

scenarios; and (iii) Type III sensors that provide information on the system-level impact (such as UAV imagery) thus allowing us to prune down the system-level impact scenarios.

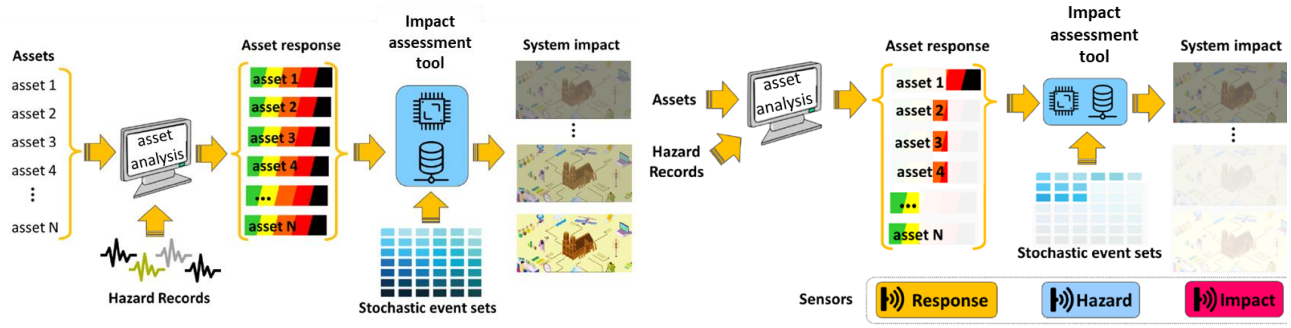

(a) (b)

Figure 1. (a) Long-term pre-event risk assessment process and (b) short-term trans/post-event scenario risk assessment process (adapted from Vamvatsikos and Chatzidaki 2022).

3 Exposure model

Within the Metsovo-Panagia segment multiple assets can be found that are vulnerable to the seismic and the wind hazards, such as tunnels, bridges, slopes, lightweight steel structures etc. In our case, to illustrate the proposed framework we focus on: (i) the slopes around the highway, one bridge founded on rock (G7), one bridge partially founded on an active landslide (G1), and the Operator Control Building (OCB), all vulnerable to seismic excitations; (ii) an ensemble of sign-support structures that are exposed to environmental conditions, thus being susceptible mainly to wind-induced fatigue damage and potentially to extreme wind actions.

The G1 bridge (Figure 2a, Mantakas et al. 2023) consists of two structurally independent twin reinforced concrete bridges, each of them carrying one travel direction. The G1 twin bridges are partially founded on an active landslide and they were constructed around 2007. The deck is supported by post-tensioned T-girder beams connected via elastometallic rubber bearings to the piers and the abutments. All piers are founded on deep foundations, either comprising groups of piles or massive caissons for the two piers that are founded within the active landslide. Thus, the caissons have a combined functionality of both protecting the bridge and stabilizing the slope. The landslide zone comprises a relatively-shallow unstable soil layer, where inclinometers and piezometers have been installed to monitor the evolution of the slope displacement. The G1 bridge and the active landslide are essentially vulnerable to the seismic action, with potential aggravation due to the water table.

The G7 bridge (Figure 2b, Giannelos and Vamvatsikos 2008) consists of two structurally independent twin bridges, each of them carrying one traffic traveling direction. The bridge was built around 2009 following the cantilever method of construction with in-situ concreting, thus the construction-phase loads govern the structural design and not the earthquake loads. The deck is a prestressed single-cell concrete box girder and it is monolithically connected to the two piers, while it is supported at each abutment via two pot bearings and a bearing with a shear key. Both piers have a hollow rectangular cross section of in-situ cast concrete and are founded within the bedrock via concrete shafts.

The OCB of the Metsovo-Panagia segment is shown in Figure 2c. It is a 2-story reinforced concrete structure of 550m^2 covered area and it houses a control center operating 24/7 with monitors displaying real-time images from the Closed-Circuit Televisions (CCTVs) of the highway, 24/7 telephone communication service, and computer equipment including the data management infrastructure.

Around the Metsovo-Panagia highway, multiple slopes can be found that can potentially be activated after earthquakes thus leading to soil and debris falling onto the highway and disrupting its regular operation. The areas of the highway where critical slopes are identified are shown in Figure 2d. Practically they comprise almost the entire length of the segment that is not a tunnel, or a bridge. Note that in general the surrounding topography is sloped from north to south, thus it is the northern lanes (i.e., the Panagia to Metsovo ones) that are in peril from rockfalls.

Finally, the steel sign-support structures of the Metsovo-Panagia segment (Figure 3a) are typically configured as portal-shaped, L-shaped, or T-shaped frames, consisting of one or two columns and a horizontal beam.

They are constructed using S275 steel, and the cross sections of their beams and columns are commonly rectangular hollow sections with added stiffeners. The columns are based on reinforced concrete foundations, while their base connection comprises a base plate welded to the column and bolted to the concrete foundation via embedded anchors. The horizontal beam is typically connected to the steel columns via end-plate connections. The shorter upper part of the column is typically is pre-welded with the beam and is connected to the rest of the column using two end-plates and pretensioned bolts, the latter aiming to increase the fatigue life of the connection.

(a) G1 bridge

(b) G7 bridge

(c) OCB

(d) debris/rockfall zones

Figure 2. (a) G1 bridge (adopted from Mantakas) et al. 2023, (b) G7 bridge, (c) operator control building and (d) highway segments that can potentially be affected if adjacent slopes are activated.

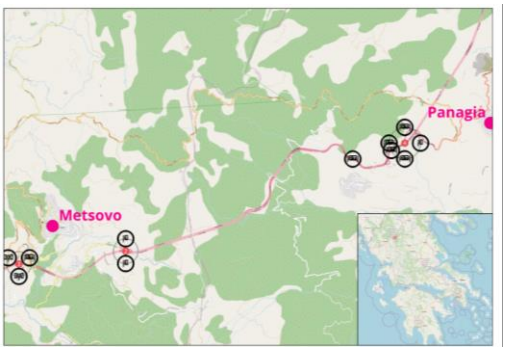

(a) OCB

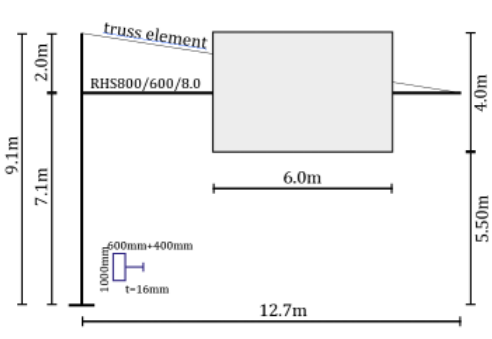

(b) L-shaped sign-support structures

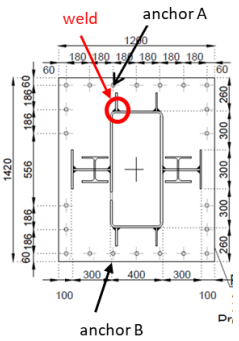

(c) column base connection

Figure 3. (a) Locations of the sign-support structures within the Metsovo-Panagia segment and (b) typical geometry of an L-shaped sign-support structure and (c) its column base connection.

4 Hazards and dependence

In our case, we focus on the seismic and the wind hazards. These are independent (Argyroudis et al. 2020) and they are not expected to affect the same assets of the highway. Thus, each hazard is treated separately and only the assets that are prone to it are considered in the corresponding analysis.

4.1 Seismic hazard assessment

The seismic hazard is assessed following the principles of Probabilistic Seismic Hazard Analysis (PSHA, Cornell 1968), by employing event-based analysis. This provides SES of thousands of seismic events that collectively represent the seismicity of the region. For each event within the SES, the spatially correlated information of the seismic hazard is defined in the form of ground motion fields. To this scope, the OpenQuake platform (Pagani et al. 2014) is used by employing the area source model of ESHM13 (Giardini et al. 2013) and the ground motion prediction equation of Boore and Atkinson (2008). Two IMs are adopted for the analysis, i.e., the peak ground acceleration (*PGA*) and the state-of-the-art average spectral acceleration, *AvgSa*, (Cordova et al., 2001):

$$AvgSa(T_{Ri}) = \left(\prod_{i=1}^{n} Sa(T_{Ri}) \right)^{1/n} \quad (1)$$

It is the geometric mean of *n* spectral acceleration ordinates, *Sa*, at periods T_{Ri}. Each *Sa* ordinate is the geometric mean of the 5%-damped spectral acceleration from the two horizontal components of each ground motion. The periods, T_{Ri}, in our case are equally spaced in [0.3s, 3.0s] with an increment of 0.1s.

4.2 Wind hazard assessment

The long-term wind hazard is assessed by employing the climatic projections of Euro-CORDEX (EC, Jacob et al, 2014) as a basis. EC models are based on alternative scenarios of greenhouse gas concentrations, named Representative Concentration Pathways (RCPs, Moss et al. 2008, Figure 4a): RCP8.5 represents a scenario of very high greenhouse gas emissions, RCP6.0 and RCP4.5 are stabilization scenarios and RCP2.6 represents a mitigation scenario of considerable negative future emission. EC provides climatic projections with a spatial resolution of ~12.5×12.5km and temporal resolution of (at least) a day, for all days up until 2100. Still, the coarse spatial and temporal resolutions of the EC data do not allow using them as a direct input for risk and resilience assessment of structures that are characterized at the level of centimeters or meters, and dynamically respond to load time-histories discretized to fractions of a second. Thus, both resolutions need to be downscaled, aiming to develop spatially and temporally correlated wind fields with a 10min time-step at all locations of interest where sign-support structures can be found.

To achieve so, the coarse EC projections are transformed to artificial spatially and temporally correlated 10min time-histories at each geolocated point of interest, named Frankenstein time-series and IM fields. To do so, a hybrid dynamical-statistical downscaling approach is employed that combines the EC projections with historical 10min weather station measurements and spatially correlated wind fields i.e., cotemporaneous wind speed and direction values at all locations of interest. These are typically derived as the product of site-specific large eddy simulations (LES) that take into account local effects and are able to provide localized wind information. For instance, a wind field for a vertical cross section along the highway around the mountains of Metsovo is presented in Figure 4b. It should be noted that the generated Frankenstein wind time-series and IM fields are not forecasts, i.e., they are not expected to be actually observed in the future, but they are plausible realizations of long-term predictions of what may happen, statistically speaking, in a future day. Although we do not necessarily believe every single 10min of the time-histories, they are expected to conform with the long-term statistics provided by EC and have the right temporal and spatial correlation to allow estimating risk in the long term for structures and infrastructure of interest to civil engineers. This process is followed for ten EC models that are based on the RCP2.6 and RCP4.5 scenarios.

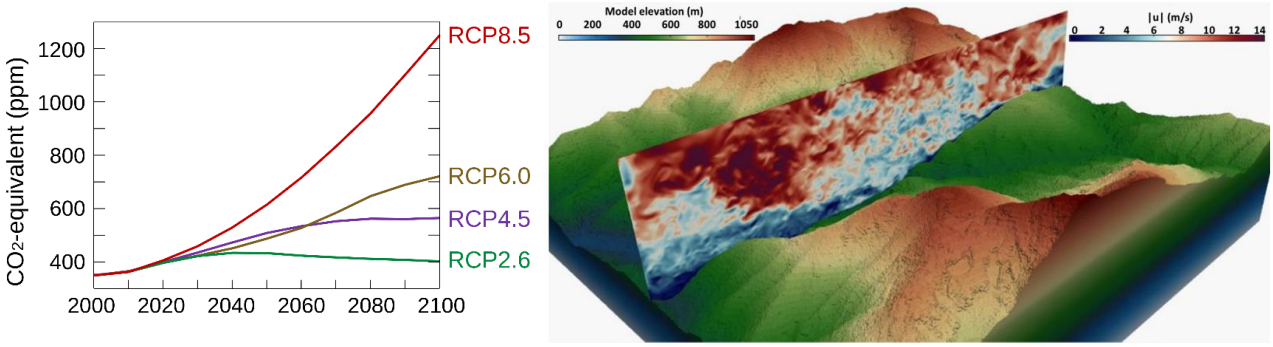

(a) (b)

Figure 4. (a) CO2-equivalent concentrations for the alternative representative concentration pathway scenarios of Euro-CORDEX (adopted from Wikipedia[1]) and (b) example of a wind field computed via LES simulations for a vertical cross section across the highway around the Metsovo valley (adopted from Hellsten et al. 2021).

5 Seismic risk and resilience assessment

The seismic risk and resilience are assessed for the entire highway by combining the seismic hazard with seismic vulnerability data for the critical highway assets. Two approaches are followed for vulnerability assessment, namely (a) component-based approach (FEMA P-58 2012) and (b) structure-level treatment. The former is employed for Tier I assets, i.e., influential ones such as the G1 and G7 bridges of our example, which require structure-specific treatment as it enables differentiating consequences to individual asset components. In our case, for the G1 bridge the critical components that are considered are the active landslide (slide), the caisson (C), the piers (P1-P7), the bearing sets at the abutments and the piers (BS1-BS9), and the expansion joints at the two abutments (EJ1, EJ2). For the G7 bridge the critical components are the pot bearings at the two abutments (PB1-PB4), the bearings with the shear keys (SK1, SK2), the expansion joints (EJ1, EJ2), the abutments themselves (A1, A2), and the piers (M1, M2). For the Tier I assets, detailed models are created and subjected to multi-stripe analysis (Jalayer and Cornell 2009) using hazard-consistent ground motion records based on the Conditional Spectrum (Lin et al. 2013). The structurally-influential components of these assets are explicitly modelled, and their response is analytically monitored during the analysis. The analysis results are combined with expert-based loss/consequence functions for each component to allow assessing vulnerability functions specific to individual components and are then combined to assess the consequences for the entire asset. On the contrary, the structure-level treatment is followed for Tier II assets, i.e., less influential ones, by employing class-generic fragility and vulnerability functions, e.g., akin to HAZUS-MH (HAZUS 2012) for which the limit-states are defined at the level of the asset (i.e., indicating global rather than local damage). These are in turn combined with expert-based damage-to-loss functions for the entire asset to offer cumulative consequences over the entire asset. This approach is followed for the OCB and the generic slopes.

By combining the consequences in terms of the number of lanes that may be closed after an event, the speed limit in the open ones, and the time needed for concluding individual component-level repair actions (for Tier I), or asset-level overall repair (for Tier II), an asset's recovery can be estimated. To this scope, a "bathtub" recovery function (Chatzidaki et al. 2020) is adopted either for individual components (Tier I) or the entire asset (Tier II). This simple shape complies with highway operator practice to remove restrictions in discrete steps, rather than in a linear or otherwise more complex manner. For Tier I assets, the recovery process of the entire asset back to full functionality is determined by overlaying the individual bathtub recovery functions of all damaged components while for Tier II assets no such granularity is possible; thus, a single bathtub function defines the recovery of the segment and all restrictions are lifted simultaneously and only when all repair actions have been concluded.

5.1 Scenario-based analysis results

An example of the system-level consequences is presented for a seismic event that is randomly selected from the SES of Section 4.1. Its magnitude is M = 6.5 and the location of its epicenter is shown in Figure 5 along

[1] https://en.wikipedia.org/wiki/Representative_Concentration_Pathway

with the associated *PGA* and *AvgSa* ground motion fields. For the given event, all generic slopes remain undamaged, while the distributions of damage for the rest of the assets appear in Figure 6; these are identical for the twin assets since they experience the same IM levels. The structure-level treatment that is employed for the OCB provides generic damage states, while the G1 and G7 bridges are treated at the component-level, offering per-component detailed results. For example, for the OCB per Figure 6c we can only tell that the slight and moderate damage states are the most frequent ones, without having any further explanation as to the reasons behind this result. Instead, for the G1 bridge, Figure 6b indicates that the most damageable components are bearings BS1 and BS9, and the landslide-prone slope itself. For the G7 bridge, Figure 6a indicates that the shear keys (SK1, SK2) are the most critical ones.

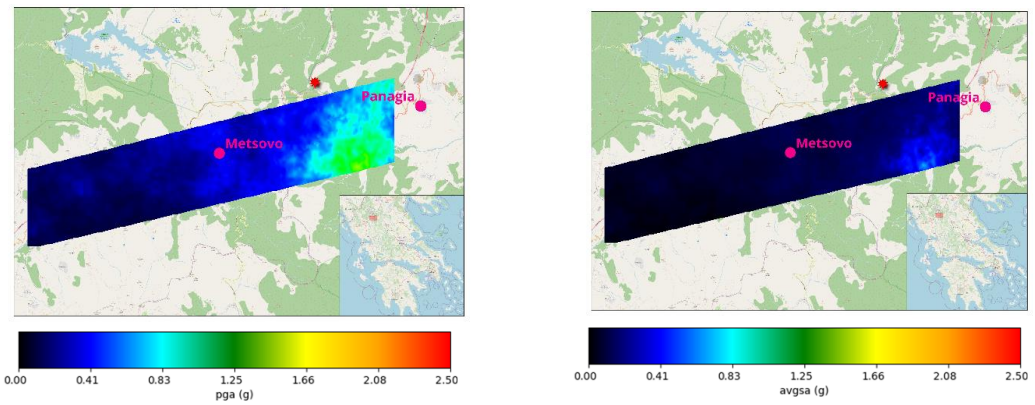

(a) (b)

Figure 5. Ground motion fields for an earthquake of magnitude M = 6.5 at the location indicated in red: (a) PGA ground motion field and (b) AvgSa ground motion field.

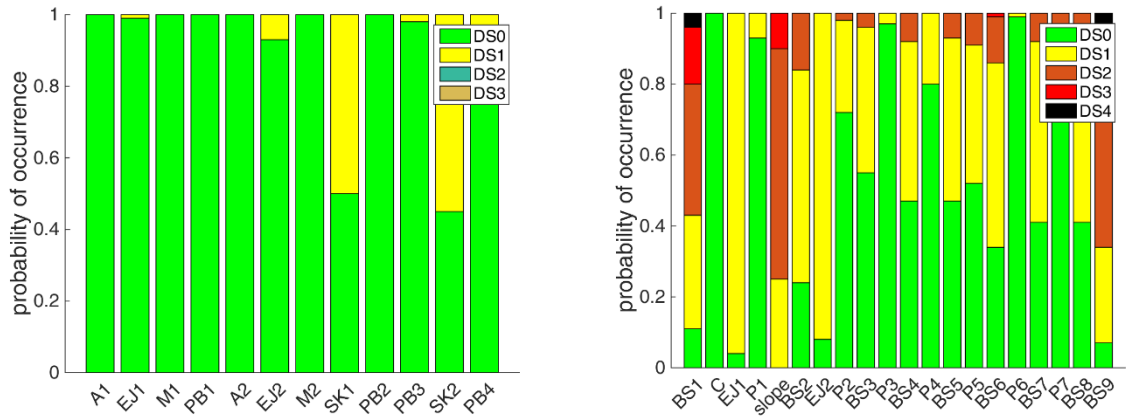

(a) damage state distribution for the components of the twin G7 bridges (b) damage state distribution for the components of the twin G1 bridges

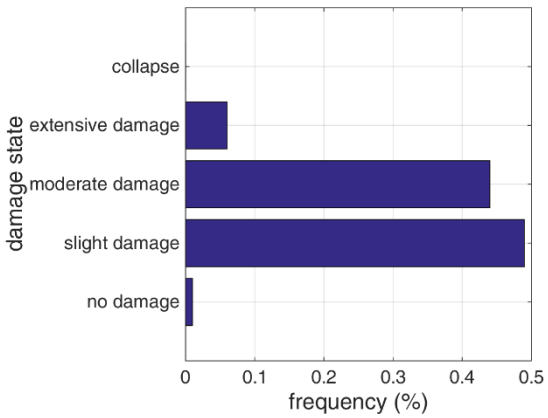

(c) damage state distribution for the OCB

Figure 6. Damage distribution for the critical highway assets for the selected event of M = 6.5.

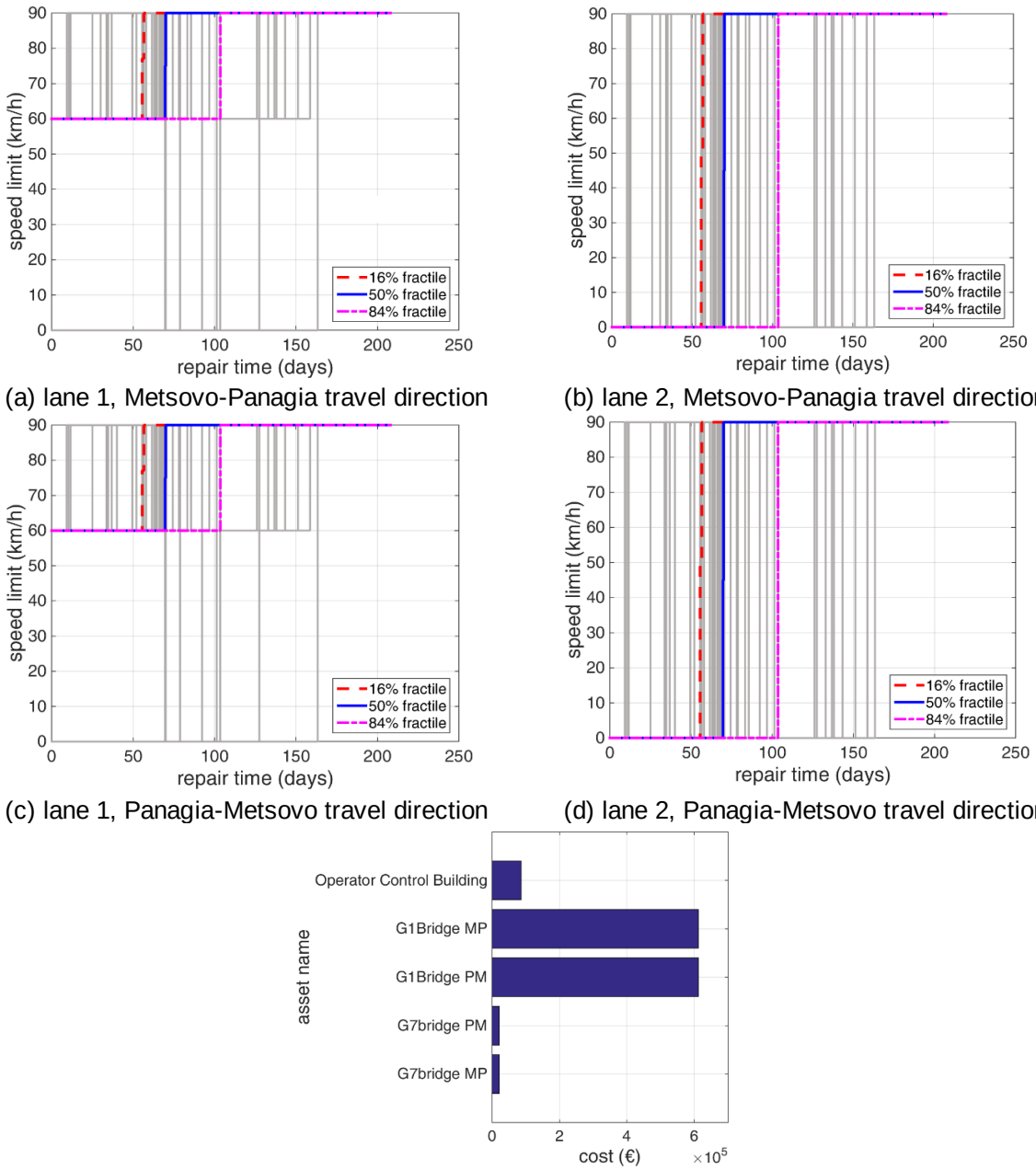

(a) lane 1, Metsovo-Panagia travel direction

(b) lane 2, Metsovo-Panagia travel direction

(c) lane 1, Panagia-Metsovo travel direction

(d) lane 2, Panagia-Metsovo travel direction

(e) average cost per critical asset

Figure 7. System-level consequences for the selected event of M = 6.5 (MP = Metsovo-Panagia, PM = Panagia-Metsovo direction). Lane 1 is the left one (i.e., the passing lane) in each direction.

The system-level recovery functions are shown in Figure 7a-d for the two lanes of the Metsovo-Panagia and of the Panagia-Metsovo travel directions. Lane 2 is on the right, and lane 1 on the left (i.e., the passing lane). It seems as if lane 1 is the one that will typically suffer the most. Actually, this is partly due to simplification. In general, one will prefer closing lane 2, since this is adjacent to the emergency lane, offering more space for parking vehicles and for storing equipment as the repairs proceed. Thus, it is the one chosen as the first to be closed by default. In reality, though, one will typically alternate closed lanes when e.g., repairing and inspecting along the length of an expansion joint. Still, this does not influence the system-level consequences (i.e., traffic throughput), only the per-lane ones. The average repair cost per asset is shown in Figure 7e, with the total loss being ~1,350,000€, allocated for repairing the damaged components of the G1 and G7 twin bridges, and the OCB.

5.2 Long-term analysis results

In order to assess long-term losses for the entire system, the scenario-based analysis is repeated for all events within the SES of Section 4.1 and the results are aggregated by accounting for the likelihood of occurrence of

each event. The outcome of this process is the loss exceedance curve of Figure 8a that provides the mean annual frequency, MAF, (or equivalently the mean return period) of exceeding any given loss value. This loss value is the direct cost for restoring the system to its pre-earthquake condition. By integrating the area below the loss exceedance curve, the average annual loss for the entire system is determined as ~6,000€; this is the amount of losses that the entire system is expected to generate on average every year due to earthquakes over a long period of time. Its low value attests to the heavy overdesign of this important infrastructure.

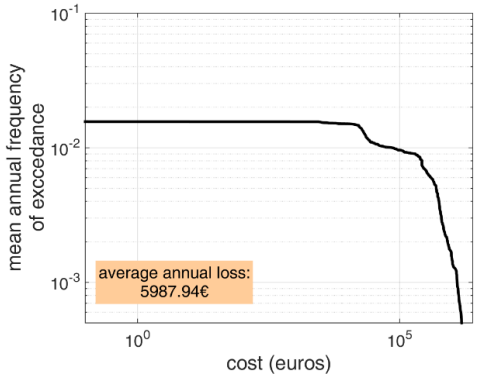

Figure 8. Loss exceedance curve for the entire system when all critical highway assets are considered.

6 Wind risk and resilience assessment

In our case, we focus on fatigue-induced damage that is caused by the wind, discounting any additional impact of vehicle-induced gusts (Li et al. 2006) due to the relatively low traffic loads of Egnatia Odos. The sign-support structures of the Metsovo-Panagia segment are located in a high-altitude environment where deicing salt is applied by the road operator for ~180 days per year in order to prevent ice formation on the road surface. The chloride ions of the deicing salt can lead to corrosion that results in reduced fatigue lifetime. Thus, the impact of corrosion in their expected fatigue lifetime is also examined.

The sign-support structures of the Metsovo-Panagia segment are classified into the Tier II category; they are grouped into three classes containing the L-shaped, T-shaped, and portal-shaped structures. The structures of the same category are assumed to have similar cross-sectional properties and dimensions, hence only an archetype structure is modelled in detail and its results are considered representative for all structures within the same class. In our case, we focus on the critical details of those structures to assess the damage accumulation due to fatigue. These are found in the column base connection and are the weld of the stiffener to the column base plate, anchor A, and anchor B, as indicatively shown in Figure 3c for the L-shaped structures. For the critical weld, only the normal stresses are considered since shear stresses are comparatively negligible; the same holds for the anchors, as they are pretensioned and only normal stresses are generated.

The damage accumulation due to fatigue for the critical details of the corroded/uncorroded sign-support structures is computed by (i) assessing the fatigue damage for the critical details of the structure on a site-agnostic basis for 10min loading intervals and (ii) combining the damage estimates with the long-term wind speed and direction Frankenstein time-series at the location of each sign-support structure to assess the damage per 10min of the time-series. Then, the long-term accumulated damage is determined. To this scope, a vector IM is adopted that comprises the 10min wind speed at 10m height, u_{10}, and the incidence angle of the wind normal to the signpost, δ.

6.1 Site-agnostic fatigue damage assessment

The site-agnostic fatigue-induced damage was assessed for the critical details of the sign-support structures found at Egnatia Odos by Ntaifoti et al. (2023). Specifically, the 3D model of each structure type was subjected to dynamic analysis using wind speed time-series as input for increased u_{10} levels and various incidence angles, δ. During the analysis, the damage due to fatigue was computed for the critical details. To achieve so, artificial wind speed time-histories were generated with a duration of 10min for increased levels of u_{10}, ranging from 1m/s to 40m/s with an increment of 1m/s. These were converted to wind pressure time-series and were applied on the 3D model of the structure, by considering 9 alternative incidence angles, δ, within the range [0°, 360°) with an increment of 45°. For each time-series, the forces at the column base connection were

computed and then converted to stresses on the critical details (i.e., anchors and welds) using simplified formulas. The rainflow counting method (Matsuishi and Endo 1968) was then employed to determine the stress ranges and the number of complete cycles given each stress range, which were then combined with the stress-life curves to allow assessing the damage due to fatigue per stress cycle. The Palmgren-Miner rule (Miner 1945) of linear damage accumulation was then employed to assess the damage on the critical details for all cycles. The same process was followed both for the uncorroded and for the corroded structures but for the latter the stress-life curves are determined based on Adasooriya et al. (2019).

In order to account for the uncertainties related to the wind loading, this process was repeated for 10 alternative wind speed time-series that were generated, thus obtaining 10 realizations of the damage accumulation due to fatigue for each (u_{10}, δ) pair. An example of the damage accumulation for anchor A and the critical weld of the L-shaped structures for wind normal to the signpost, i.e., $\delta = 0°$, is shown in Figure 9, both for the corroded and the uncorroded cases. Overall, the fatigue-induced damage accumulation per (u_{10}, δ) pair is greater for the corroded than the uncorroded structure, and for the weld rather than the anchor.

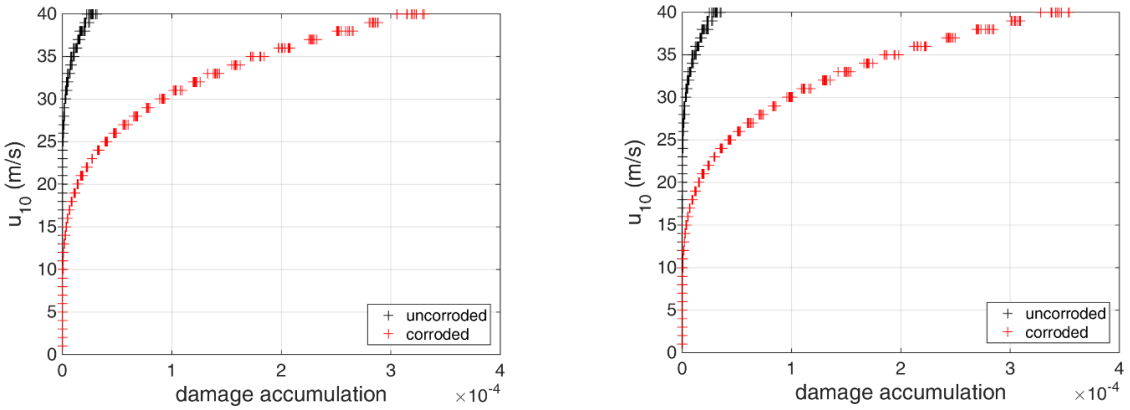

(a) anchor A (b) weld

Figure 9. Fatigue damage at (a) anchor A and (b) the critical weld of the L-shaped sign-support structures for wind acting normal to the signpost.

6.2 Long-term damage accumulation due to fatigue

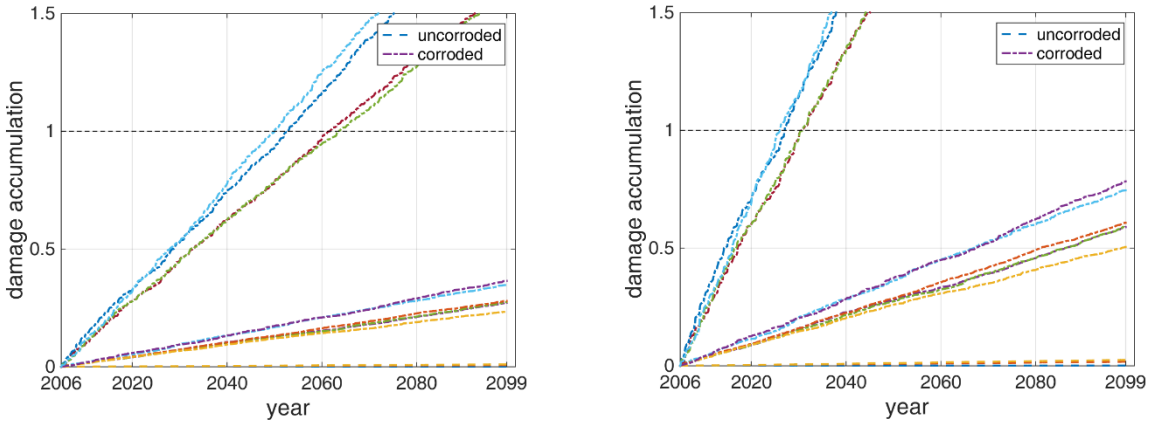

(a) anchor A (b) weld

Figure 10. Fatigue-induced damage accumulation for the critical details of an L-shaped sign-support structure of the Metsovo-Panagia segment: (a) anchor A, and (b) weld.

The 10min damage data are combined with site-specific Frankenstein time-series of Section 4.2 to assess the long-term damage accumulation due to fatigue by considering also the impact of climate change. Specifically, for each asset and 10min interval of the Frankenstein time-series, the 10min fatigue damage at the critical details is assessed based on the corresponding analysis results. By aggregating the 10min damage values for all 10mins over the years, the cumulative damage over time can be determined. The results are indicatively presented in Figure 10 for an L-shaped sign-support structure of the Metsovo-Panagia segment that is assumed to be installed around 2006, i.e., when the Metsovo-Panagia segment was at the final stages of

construction. Thus, the accumulated damage due to fatigue from 2006 up to 2100 for all examined climate change scenarios is shown both for the corroded and the uncorroded structures. It can be observed that the damage accumulation due to fatigue for the uncorroded structure is minor as even by 2100 the cumulative value remains lower than the Palmgren-Miner threshold of 1.0. For the corroded asset, 4 out of the 10 examined climate change scenarios lead to crack initiation around 60 years after installation, with the most critical component being the weld. It should be noted that these outcomes are derived by assuming that the structures are in a corroded state since their installation, which is typically conservative, but not necessarily far off if maintenance is not up to par.

7 Conclusions

The HAPI risk and resilience assessment framework is employed for assessing risk and resilience for the Metsovo-Panagia segment of the Egnatia highway in Greece, focusing on the seismic and wind hazard. This framework can be applied for assessing consequences for individual highway/road infrastructure assets while the combined results can offer an accurate and unbiased risk and resilience assessment of interconnected road infrastructure and provide an integrated view of the overall system resilience. The framework can be considered as quite straightforward, still the challenge is the definition of hazard as well as the limit states and associated consequences on an asset-by-asset and system-level basis. This requires the assistance of engineers specialized in the design and construction of similar structures as well as of road operators experienced in road maintenance, repair, and rehabilitation actions. After delineating the damage states and consequences, the impact and overall resilience associated to any catastrophic event can be can be reliably quantified.

8 Acknowledgments

The first author gratefully acknowledges the financial support provided by the Eugenides Foundation in Greece (scholarship for doctoral studies in NTUA grant). Financial support has also been provided by EU project “PLOTO– Deployment and Assessment of Predictive modelling, environmentally sustainable and emerging digital technologies and tools for improving the resilience of IWW against Climate change and other extremes”, Grant Agreement number 101069941.

9 References

Adasooriya N., Pavlou D., Hemmingsen T. (2019). Fatigue strength degradation of corroded structural details: A formula for S-N curve. *Fatigue and Fracture of Engineering Materials and Structures*, 43: 721-733

Argyroudis S.A., Mitoulis S.A., Hofer L., Zanini M.A., Tubaldi E., Frangopol D.M. (2020). Resilience assessment framework for critical infrastructure in a multi-hazard environment: Case study on transport assets. *Science of the Total Environment*, 714: 136854.

Ayyub B.M., McGill W.L., Kaminskiy M. (2007). Critical asset and portfolio risk analysis: An all-hazards framework. *Risk Analysis: An International Journal*, 27(4): 789-801

Boore D.M., Atkinson G.M. (2008). Ground-motion prediction equations for the average horizontal component of PGA, PGV, and 5%-damped PSA at spectral periods between 0.01 s and 10.0 s. *Earthquake Spectra*, 24 (1): 99-138

Chatzidaki A., Bakalis K., Vamvatsikos D. (2020). Seismic resilience assessment for the G7 highway bridge in Greece. Proceedings of the XI International Conference on Structural Dynamics, Athens, Greece

Cordova P., Deierlein G., Mehanny S.F., Cornell C.A. (2001). Development of a two-parameter seismic intensity measure and probabilistic assessment procedure. The Second U.S.-Japan Workshop on Performance-Based Earthquake Engineering Methodology for Reinforced Concrete Building Structures, Sapporo, Hokkaido, Japan.

Cornell C.A. (1968). Engineering seismic risk analysis. *Bulletin of the Seismological Society of America*, 58: 1583-1606

Costa C., Figueiredo R., Silva V., Bazzurro P. (2020). Application of open tools and datasets to probabilistic modeling of road traffic disruptions due to earthquake damage. *Earthquake Engineering and Structural Dynamics*, 49(12): 1236-1255.

Dong Y., Frangopol D.M. (2015). Risk and resilience assessment of bridges under mainshock and aftershocks incorporating uncertainties. *Engineering Structures*, 83: 198-208.

Faturechi R., Miller-Hooks E. (2014). Travel time resilience of roadway networks under disaster. *Transportation research part B: methodological*, 70: 47–64

FEMA (2012). Seismic Performance Assessment of Buildings, Volume 1 – Methodology. Report FEMA P58-1, Federal Emergency Management Agency, Washington, DC.

Giannelos C., Vamvatsikos D. (2008). Simplified methods of nonlinear dynamic analysis of a bridge under bi-directional seismic loading. Proceedings of the 3rd Panhellenic Conference on Earthquake Engineering and Engineering Seismology, Athens, Greece.

Giardini D., Woessner J., Danciu L., Crowley H. et al. (2013). Seismic Hazard Harmonization in Europe (SHARE): Online Data Resource, http://www.share-eu.org/node/61.html

HAZUS (2012). Hazus–MH 2.1: Technical manual. Washington, DC, USA.

Hellsten A., Auvinen M., Barmpas F. (2021). D3: D3.3.1 Report on the dynamical downscaling of climate and atmospheric impacts V1. The PANOPTIS project, GA: 769129

Jacob D., Petersen J., Eggert B., Alias A., et al. (2014). EURO-CORDEX: new high-resolution climate change projections for European impact research. *Regional Environmental Changes*, 14(2): 563-578

Jalayer F., Cornell C.A. (2009). Alternative non-linear demand estimation methods for probability-based seismic assessments. *Earthquake Engineering and Structural Dynamics*, 38(8): 951-972

Kappos A., Sextos A., Stefanidou S., Mylonakis G., Pitsiava M., Sergiadis G. (2014). Seismic risk of inter-urban transportation networks. *Procedia Economics and Finance*, 18: 263-270

Kiremidjian A., Moore J., Fan Y.Y., Yazlali O., Basoz N., Williams M. (2007). Seismic risk assessment of transportation network systems. *Journal of Earthquake Engineering*, 11(3): 371-382

Li X., Whalen T.M., Bowman M.D. (2006). Fatigue strength and evaluation of sign structures, Volume 1: Analysis and evaluation. Joint Transportation Research Program, 261

Lin T., Harmsen S.C., Baker J.W., Luco N. (2013). Conditional spectrum computation incorporating multiple causal earthquakes and ground-motion prediction models. *Bulletin of the Seismological Society of America*, 103(2A): 1103-1116

Mantakas A., Tsatsis A., Loli M., Kourkoulis R., Gazetas G. (2023), Seismic response of a motorway bridge founded in an active landslide: a case study, *Bulletin of Earthquake Engineering*, 21(1): 605-632.

Markolf S.A., Hoehne C., Fraser A., Chester M.V., Underwood B.S. (2019). Transportation resilience to climate change and extreme weather events–Beyond risk and robustness. *Transport Policy*, 74: 174-186.

Miner M.A. (1945). Cumulative damage in fatigue. *Journal of Applied Mechanics*, 12(3): A159-A164

Moss R.H., Babiker M., Brinkman S., et al. (2008). Towards new scenarios for analysis of emissions, climate change, impacts, and response strategies (No. PNNL-SA-63186). Pacific Northwest National Lab.(PNNL), Richland, WA (United States).

Ntaifoti A., Chatzidaki A., Gantes C., Vamvatsikos D. (2023). Corrosion influence on fatigue resistance of lightweight steed structures. Proceedings of the 10th National Conference of Steel Structures, Athens, Greece

Pagani M., Monelli D., Weatherill G.A., Garcia J. (2014). The OpenQuake-engine Book: Hazard. Global earthquake model (GEM) technical report 2014-08

Vamvatsikos D., Chatzidaki A. (2022). The HAPI sensor-aware framework for infrastructure risk and resilience assessment. Proceedings of the 3rd International Conference on Natural Hazards & Infrastructure ICONHIC 2022, Athens, Greece.

Werner S.D., Taylor C.E., Moore J.E., Walton J.S., Cho S. (2000). A risk-based methodology for assessing the seismic performance of highway systems. Report MCEER-00-0014, Multidisciplinary Center for Earthquake Engineering Research, University at Buffalo

Matsuishi M., Endo T. (1968). Fatigue of metals subjected to varying stress. *Japan Society of Mechanical Engineers*, 68(2): 37-40.